



COMPOSITE MATERIALS FOR SUSTAINABLE AND ECO-FRIENDLY MATERIAL DEVELOPMENT AND APPLICATION

Effect of Thermo–Processing on the Microstructure, Impact Abrasion Wear, and Corrosion Resistance Properties of TiC Reinforced Al-Added High-Mn Steel Matrix Composite

RENUPRAVA DALAI,¹ SUDIPTA MOHAPATRA,¹ SIDDHARTHA DAS,¹
and KARABI DAS ^{1,2}

1.—Department of Metallurgical and Materials Engineering, Indian Institute of Technology, Kharagpur 721302, India. 2.—e-mail: karabi@metal.iitkgp.ac.in

The present work aims to study the effect of thermo–mechanical processing on the microstructure, impact abrasion wear, and corrosion resistance properties of a Fe-17Mn-3Al (wt.%) steel matrix composite reinforced with 10 wt.% TiC, synthesized by the conventional melting and casting route. The high-manganese steel matrix composite (HMSMC) was homogenized at 1100°C for 1 h followed by forging with a 50% reduction in thickness. Then, the steel was subjected to warm rolling at 1100°C to achieve a 30% reduction in thickness followed by annealing at 800°C. In this work, the applied thermo–mechanical processing of the investigated HMSMC consists of forging, warm rolling, and annealing at 800°C. The XRD patterns of the homogenized and thermo–mechanically processed HMSMC show the presence of α -ferrite, γ -austenite, and TiC phases. In addition, the SEM micrographs corroborate the presence of ferrite in the inter-dendritic region, austenite in the dendritic region, large TiC particles in the inter-dendritic region, and small TiC particles in the dendritic region. Thermo–mechanical processing improves the density, hardness, impact abrasion wear (IAW) resistance, and corrosion resistance of the HMSMC. The improvement in properties is due to the thermo–mechanical processing which closes the pores and microvoids.

INTRODUCTION

High-manganese steel (HMS) is suitable for mining equipment, like crusher plates, and mineral processing equipment, like grinding mills, due to its high work-hardening rate and wear-resistant property. The HMS exhibits this high wear resistance and rate of work hardening only under high-impact loading and stress conditions.^{1–3} As a result, there are demands from industries to modify the microstructure and the mechanical and tribological (wear and corrosion) properties of HMS to improve the working life of the mining and mineral equipment that can work more efficiently under both low- and high-impact loading conditions. Many researchers have studied the wear properties of HMS by

adding alloying elements like Cr, Nb, and Ti, altering the Mn and C percentages, and reinforcing it with hard ceramic particles like TiC, (Ti,W)C, VC, WC, TiN, etc. Among these alternatives, ceramic particle reinforcement in HMS to develop high-manganese steel matrix composites has been a research interest for the last two decades. Because it provides excellent mechanical and tribological properties.^{4–11} Zhang et al. coated the surface of the HMS with a WC-HMS composite using the centrifugal casting method. They observed (Ti,W)C precipitation of carbides like $\text{Fe}_3\text{W}_3\text{C}$ or M_{23}C_6 during annealing at 1000°C. This precipitate formed a stronger interfacial bond between the HMS and WC particles and enhanced the impact abrasion wear (IAW) resistance of the HMS by developing an HMS matrix composite (HMSMC).¹² Song and Zhang developed a WC-reinforced HMSMC with a centrifugal casting technique. Reinforcement of WC particles improved the IAW resistance of the

(Received January 31, 2023; accepted June 19, 2023; published online July 17, 2023)

HMS.¹³ Moghaddam et al. developed an in situ VC-reinforced HMSMC using the conventional melting–casting method. According to their observation, HMSMC provides higher IAW resistance than HMS. The increased hardness, strength, and reduced contact area between the steel matrix abrasive particles made the surface more difficult for plastic flow.¹⁴ You-ping et al. reinforced TiN particles in HMS using the vacuum evaporation casting method. They revealed that the reinforced TiN particles were uniformly present in the matrix. The developed HMSMC showed better IAW resistance than the HMS.¹⁵ Dalai et al. studied the effect of TiC on the IAW resistance of HMSMC (Fe17Mn10TiC). They reported that the reinforcement of TiC increased the impact abrasion wear resistance of the composite.¹⁶ Luo et al. developed TiC-reinforced HMSMC and found that its wear rate was lower than that of HMS.¹⁷ Qiu et al. and Almanor et al. incorporated nanosized TiC particles into a steel matrix to significantly improve the properties of the composite.^{18,19} However, no research work is available on the IAW resistance of Al-added TiC reinforced HMS.

The Al addition enhances the work-hardening rate and high-stress abrasion resistance in HMS by suppressing the carbon activity and diffusivity.²⁰ According to Abbasi et al., the presence of Al in HMS improved the yield strength.²¹ Us Shon et al. studied four HMS and reported that the presence of Al, a ferrite stabilizer in HMS, enhanced the Charpy impact energy.²² The alloying element Al improved the low-stress abrasive wear resistance of HMS.²³ In Fe–C steels, 1 wt.% of Al decreased the density and Young's modulus values by 1.3% and 2%, respectively.²⁴ The addition of Al to HMS (Fe–17Mn) reduced the hardness and elastic modulus but increased the impact energy.²⁵ The presence of hard TiC particles and lighter Al makes the HMSMC a highly IAW-resistant material due to its high strength, hardness, and toughness. However, HMSMCs are more prone to corrosion when exposed to a corrosive environment for a longer duration, and pits are formed mainly at the interface between the reinforcement and matrix. The rate of galvanic corrosion is faster due to the formation of more galvanic cells between the austenite matrix and the TiC reinforcement.^{26,27} However, during corrosion, the presence of Al is beneficial because it forms a protective oxide layer of Al₂O₃, which enhances the corrosion resistance properties of the Al-added steel and composites.²⁸ These tribological properties of HMSMC were further improved using the forming or thermo-mechanical processing methods.^{29–32} Hence, the objective of the present work is to study the effect of thermo–mechanical processing on the microstructure, impact abrasion wear resistance, and corrosion resistance properties of an Al-added TiC reinforced HMSMC.

MATERIALS AND METHODS

Processing of the HMSMC

The conventional melting–casting route was used to synthesize a HMSMC containing 10 wt.% TiC, 3 wt.% Al, and 17 wt.% Mn, with the balance of Fe. According to the stoichiometric calculation, initially, the calculated amount of raw materials, such as steel scrap and cast iron, were heated to 1600°C and held for 15 min at this temperature, and then the required amounts of electrolytic manganese and aluminum were added to the melt. Then, using the plunging method, ferrotitanium was introduced into the melt at 1625°C. In this process, a continuous stirring of the melt with an iron rod helped to obtain a homogenous melt and uniformly distributed the TiC particles. In the present work, to get a faster cooling rate, the melt was poured into a metallic mold to solidify the developed HMSMC.

The HMSMC was homogenized at 1100°C for 1 h followed by forging to reduce the thickness by 50%. The forged samples were then subjected to rolling at 1000°C followed by annealing at 800°C which achieved a 30% reduction in thickness to complete the thermo–mechanical process.

Characterization and Testing of HMSMC

Phase identification of the HMSMC was carried out by X-ray diffraction (XRD; D8 Advance diffractometer; Bruker) with Co-K α radiation, wavelength 1.79 Å, scan range 20°–120°, and step size 0.02°. A scanning electron microscope (SEM; Quanta 250 FEG; FEI) equipped with energy-dispersive X-ray spectroscopy (EDS; Bruker) analyzed the microstructures of the HMSMC samples after paper- and cloth-polishing followed by etching with 2% Nital solution. Archimedes' principle was used to determine the density of the composite samples.

Impact Abrasion Wear Test

An IAW testing machine (DUCOM TR56-M3) was used to determine the IAW resistance of the composite samples. Figure 1 shows a schematic of the IAW testing machine. In the IAW test, the treated composite samples were the testing samples that acted as the upper sample, which continuously impacted the surface of a lower-rotating steel disk. A continuous flow of the abrasive particles, i.e., sand, was allowed onto the contact surface between the upper and lower samples, and due to this, IAW occurs on the composite sample surface. Here, the weight loss or material loss method determines the amount of wear loss for the treated composite samples. Table I shows the IAW testing parameters used in the present work.

Electrochemical Corrosion Test

An Autolab PG Stat-30 (Potentiostat/Galvanostat) machine was used for electrochemical

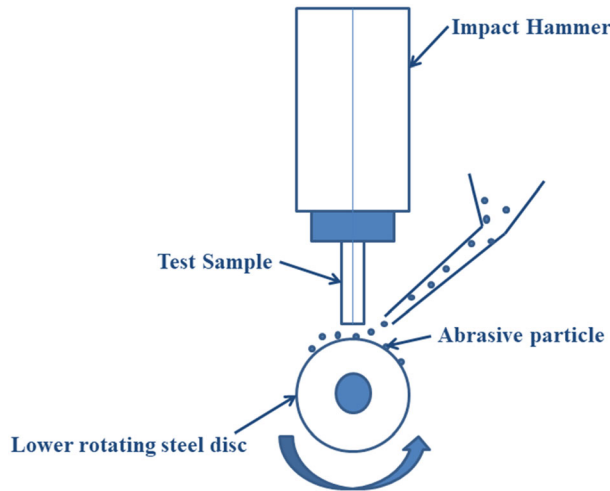


Fig. 1. Schematic illustration of the IAW testing machine.

Table I. IAW test parameters

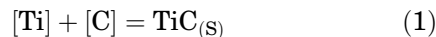
HMSMC dimension (L × W × T)	(30 mm × 10 mm × 10 mm)
Lower disc rotation speed	200 rev min ⁻¹
Test duration	0–8 hr
Impact energy	0.7 J
Abrasive medium	Quartz
The flow rate of the abrasive medium	304 g min ⁻¹

measurements with a galvanostatic DC power supply to measure the corrosion rate of the HMSMC samples at room temperature in a 3.5% NaCl solution. The samples were mirror-polished before the corrosion test. A standard three-electrode configuration with a counter electrode (99% pure platinum), a reference electrode (Ag/AgCl/3.0 M KCl), and a working electrode (homogenized and thermo-mechanically processed HMSMC sample) was used in the present investigation. A surface area of 1 cm² of the sample surface was exposed to an electrolyte of 3.5% NaCl aqueous solution.³³

RESULTS AND DISCUSSION

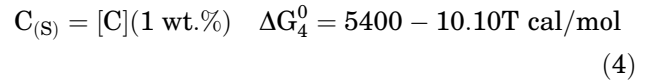
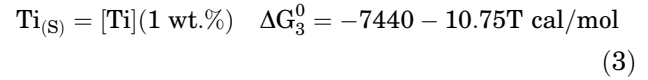
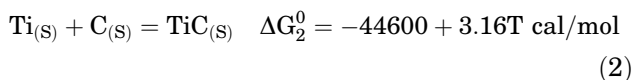
Formation of TiC Particles

TiC particles form in an iron-based alloy solution by a reaction between Ti and C:³⁴



where [Ti] and [C] are Ti and C in solution, respectively.

Equation 1 can be obtained from Eqs. 2, 3, and 4.^{35,36}



$$\text{Equation 1} = [\text{Equation 2}] - [\text{Equation 3}] - [\text{Equation 4}]$$

Therefore, the standard free energy for TiC formation in liquid iron is $\Delta G_1^0 = -42,560 + 24.01T$ cal/mol considering the standard state of Ti and C as 1 wt.% solution.

From the above equation, it is revealed that TiC particles can form at a temperature which is lower than 1500°C. Hence, a supersaturated solution of Ti and C in liquid iron forms at 1610°C, which is the liquid melt holding temperature. During cooling, the solubility of both Ti and C in the Fe decreases which results in the formation of TiC by Eq. 1.

Microstructural Characterization

Figure 2 shows the low- and high-magnification SEM micrographs of the homogenized and thermo-mechanically processed HMSMC sample. Figure 2a reveals the inter-dendritic region A (α -ferrite) and the dendritic region B (γ -austenite) of the homogenized HMSMC. The small TiC particles are nucleated from the solid state, but the large TiC particles are from the liquid melt.¹⁶ The SEM micrographs confirm that the TiC particles are mainly present in the inter-dendritic region. Figure 2b shows that thermo-mechanical processing removes the dendrites from the homogenized samples, while Fig. 2c shows the higher-magnification SEM image of Fig. 2a in which dendrites are visible. The small and large TiC particles are distinguished with the help of a higher-magnification SEM image (Fig. 2d). The EDS maps of the homogenized and thermo-mechanically processed HMSMC are depicted in Fig. 2e and f, respectively.

Figure 3 shows the EDS analysis of the inter-dendritic and dendritic regions marked by the thermo-mechanically processed HMSMC. The point EDS measurements of the inter-dendritic and dendritic regions were determined to know the mass fraction (%) of Al, Mn, Ti, and Fe. The amount of Mn is slightly higher and Al is slightly lower in the dendritic region because austenite is present. Similarly, in the inter-dendritic region, the amount of Mn is slightly lower and Al is slightly higher because ferrite is present. However, no significant difference was observed in the values of Mn and Al in the inter-dendritic and dendritic regions of the HMSMC samples.

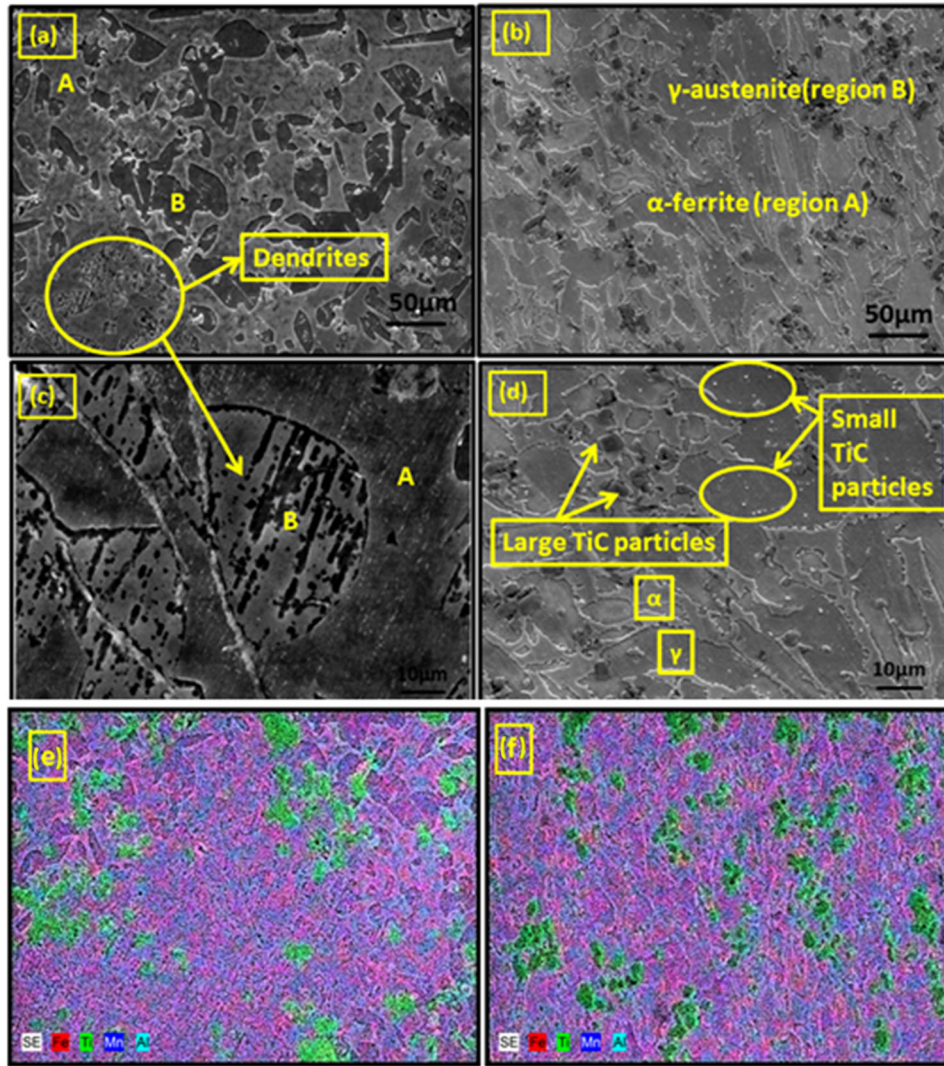


Fig. 2. SEM micrographs of (a) homogenized HMSMC (inter-dendritic region marked as A, dendritic region marked as B) (b) thermo-mechanically processed HMSMC, (c and d) higher magnification images of (a) and (b), respectively, (e and f) EDS color mapping of homogenized and thermo-mechanically processed HMSMC, respectively.

Figure 4 shows the XRD plots for the homogenized and thermo-mechanically processed HMSMC samples, confirming the presence of α -ferrite, γ -austenite, and TiC for both composite samples.

Density and Hardness Measurement

Table II lists the density and hardness values of the HMSMC samples. Thermo-mechanical processing helps to improve the density values from 6.9 g/cm^3 to 7.12 g/cm^3 by removing the pores, and also improves the hardness of the solutionized HMSMC. According to Table II, there was an improvement of 22 HV after thermo-mechanical processing. An increase in density value along with the microstructural refinement and some residual rolling strain may have contributed to the hardness increment in thermo-mechanically processed samples.

Impact Abrasion Wear (IAW)

Figure 5 shows the IAW test results of the HMSMC-treated samples. As the IAW testing time increases from 2 h to 8 h, the material loss from the sample surfaces increased for both the HMSMC samples. During the impact abrasion wear process, a microcrack nucleates when the stress concentration reaches a critical value. Then, there is a growth of the microcrack that generates spalling pits on the HMSMC surface, which is the reason for the loss of material from the composite sample surfaces. The higher hardness of the thermo-mechanically treated HMSMC sample results in less material loss.

Figure 6 depicts the surface morphologies of the treated HMSMC sample after the IAW test. After 2 h of testing, the homogenized HMSMC sample surface consists of only large micro-cutting grooves

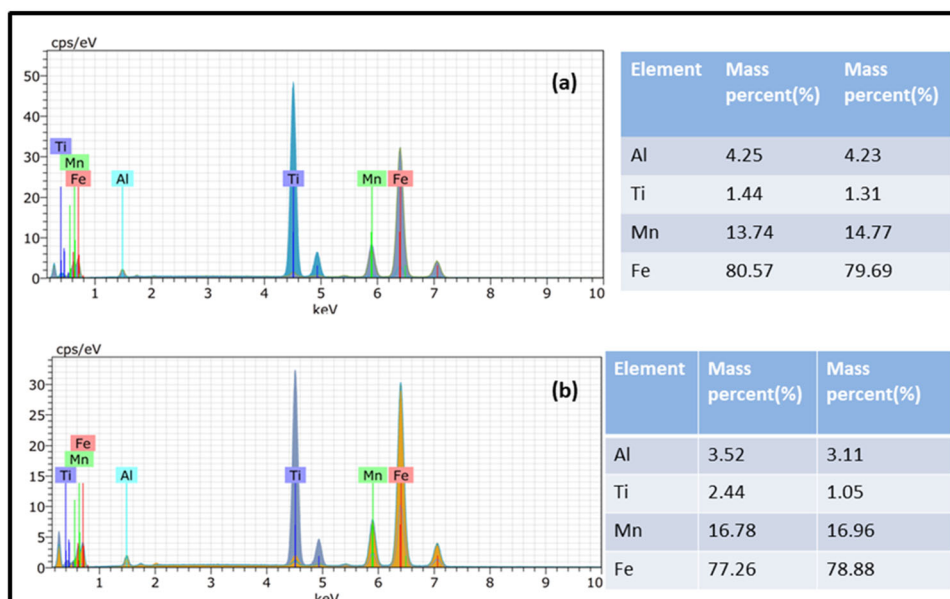


Fig. 3. EDS analysis of (a) inter-dendritic region marked as A (Fig. 2) and (b) dendritic region marked as B (Fig. 2) of the homogenized and thermo-mechanically processed HMSMC.

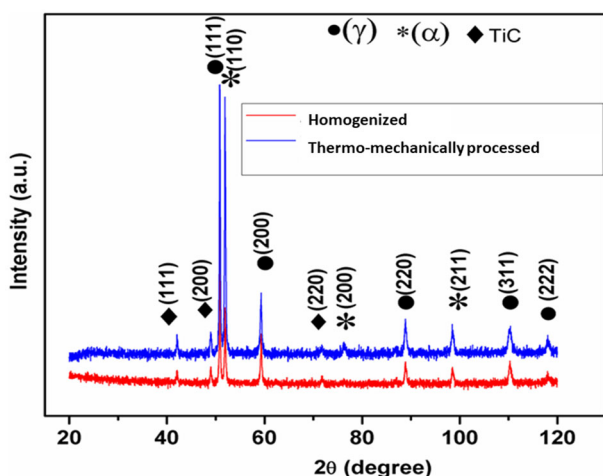


Fig. 4. XRD pattern of the HMSMC samples.

Table II. Density and hardness values of the treated HMSMC samples

Sample	Density(g/cm ³)	Hardness(HV)
Homogenized HMSMC	6.9	257 ± 4
Thermo-mechanically processed HMSMC	7.12	279 ± 7

(Fig. 6a), but the thermo-mechanically processed HMSMC sample surface shows the presence of small micro-cuttings (Fig. 6b) after 2 h of testing. However, after 8 h, the homogenized HMSMC shows deep micro-cutting grooves and spalling craters on the sample surface (Fig. 6c). Figure 6d

reveals that after 8 h of the IAW test, the thermo-mechanically processed HMSMC sample surface consists of a mechanically mixed layer. During the impact wear process, the spalling pits and craters remove some material from the HMSMC sample surfaces, and these worn-out materials form a mechanically mixed layer at the surface of the HMSMC sample due to the longer duration test.

In the present investigation, using the Stata 13 software, *t* test results (mean difference test) were analyzed for the impact-abrasion wear test. Tables III and IV present the *t* test results for the homogenized and thermo-mechanically processed HMSMC samples. which show that, when the time was less than 4 h, the mean weight loss was 0.449 mg, and when the time was more than 4 h, the mean weight loss was 0.642 mg, which is statistically different. In the case of a thermo-mechanically processed HMSMC sample, when the time was less than 4 h, the mean weight loss was 0.4115 mg, and when the testing time was more than 4 h, the mean weight loss was 0.612 mg, which is statistically significant and different. The *t* test results suggest that the weight loss is less for the thermo-mechanically processed HMSMC than for the homogenized HMSMC. For both the treated HMSMC, the weight loss was less for 0–4 h than for 4–8 h.

Corrosion Resistance Measurement

Figure 7 shows the potentiodynamic polarization curves of the HMSMC samples. Current density is an important parameter for measuring the rate of corrosion, and Fig. 7 shows that the greater the current density, the more will be the charge transfer, resulting in accelerated corrosion. Equation 5

represents the Stern–Geary equation to determine the corrosion current density:²⁶

$$I_{corr} = \frac{1}{2.303R_p} \left(\frac{b_a \times b_c}{b_a + b_c} \right) \quad (5)$$

where the corrosion current density (I_{corr}) is in amps/cm^2 , the polarization resistance (R_p) is in ohms/cm^2 , and b_a and b_c are the anodic and cathodic Tafel slopes in volts/decade of current density, respectively. The rate of corrosion in mm/year is determined from Eq. 6:

$$\text{Corrosion rate} = \frac{CWI_{corr}}{\rho} \quad (6)$$

where C is the conversion factor, W is the equivalent weight in g , and ρ is the density of the material in g/cm^3 .

Table V sets out the values of the corrosion potential (E_{corr}), the corrosion current density (I_{corr}), and the corrosion rate of the composite samples obtained from the polarization curves. A higher negative corrosion potential indicates a higher corrosion rate.³⁷ Hence, the thermo–mechanically processed HMSMC sample provides higher corrosion resistance than the homogenized sample.

Figure 8 shows the SEM micrographs of the HMSMC sample surfaces after the potentiodynamic polarization tests in an aqueous solution containing 3.5% NaCl. Figure 8a and b confirms the presence of corrosion products in the HMSMC samples. Homogenization of the HMSMC only dissolves the $(\text{FeMn})_3\text{AlC}$ carbides present in the as-cast composite. When the Al-containing steel or composite is exposed to the corrosion atmosphere, Al generally forms a protective oxide layer of Al_2O_3 , which enhances the corrosion resistance properties of the Al-added steel and composites. However, thermo–mechanical processing improves corrosion resistance by closing up the defects like microvoids in the matrix and at the particle–matrix interface. Hence, the thermo–mechanically processed HMSMC sample has higher corrosion resistance than the homogenized HMSMC sample. Nie et al. deformed an Al-TiB₂/TiC composite for 20%, 40%, 80%, and 90%, and suggested that a moderate amount of reduction during rolling (20%) only

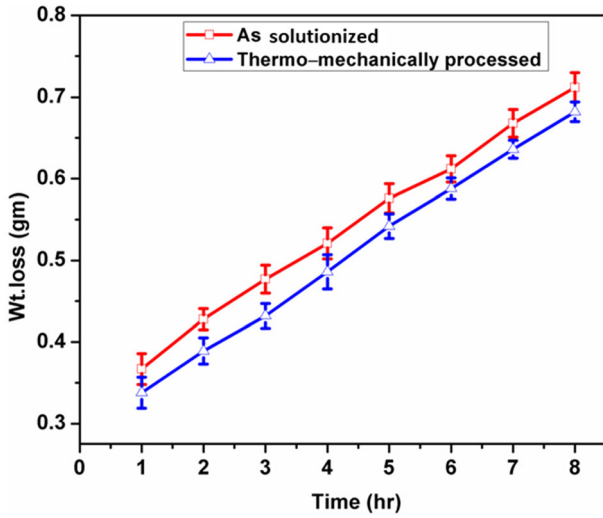


Fig. 5. Graph showing Wt. loss versus testing time of the treated HMSMC samples.

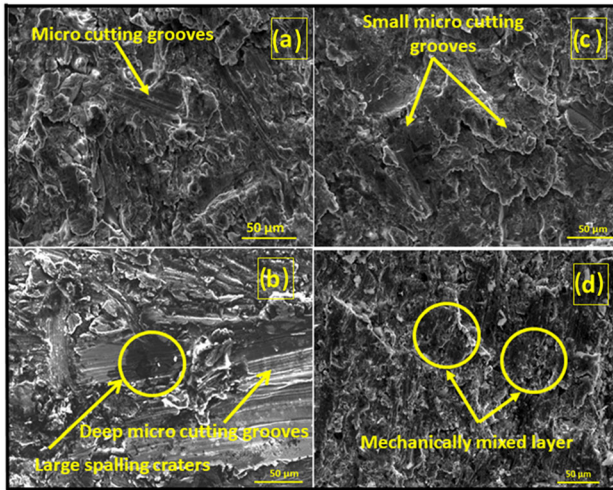


Fig. 6. SEM micrographs of the worn surface of as-homogenized HMSMC sample after (a) 2 h and (b) 8 h, and thermo–mechanically processed HMSMC sample after (c) 2 h (d) 8 h.

Table III. T-test with equal variances (Homogenized)

	Obs1	Obs2	Mean1	Mean2	Dif	St_Err	t_value	p_value
Wt. loss (mg)	0–4 h	4–8 h	0.449	0.642	0.194	0.044	4.35	0.005

Table IV. T-test with equal variances (Thermo–mechanically processed)

	obs1	obs2	Mean1	Mean2	Dif	St_Err	t_value	p_value
Wt. loss (mg)	0–4 h	4–8 h	0.4115	0.612	0.2005	0.0435	4.6	0.0035

modified the interfaces between the matrix and particles, which helped to improve the corrosion resistance. They also point out that a higher amount of deformation generated stress concentrations leading to a higher corrosion rate for the composite

materials.³⁸ Figure 8c and d shows the homogenized and thermo-mechanically processed HMSMC samples, respectively, after the removal of the corrosion product. Pits are formed on the sample surface of both samples due to corrosion. However, the homogenized sample (Fig. 8c) surface due to a higher corrosion rate contains a larger number of pits than the thermo-mechanically processed sample (Fig. 8d).

Figure 9 shows the corrosion mechanism for the HMSMC immersed in an aqueous solution containing 3.5% NaCl. The presence of Al in the HMS generally develops a protective oxide layer that protects the steel from the corrosion environment.^{39,40} In the present work, the developed HMSMC contains 3 wt.% of Al, which develops a protective oxide layer, however, this becomes weaker due to microvoids, impurities, and discontinuities if present on the composite sample surface when exposed to the corrosion environment for a longer duration. The homogenized HMSMC sample shows the presence of microvoids (Fig. 9a), and these reduce the corrosion resistance of the HMSMC. The Cl⁻ ions first accumulate in the microvoids and lower the pH value,⁴¹ then they hinder the formation of the oxide film at the matrix-

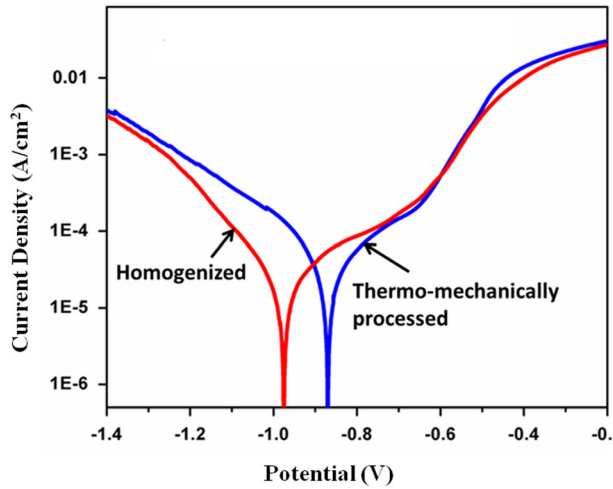


Fig. 7. Potentiodynamic polarization curves of the HMSMC samples.

Table V. The electrochemical parameters of the HMSMC samples

Sample	E_{corr} (V)	I_{corr} (A/cm ²) × 10 ⁻⁶	Corrosion rate (mm/year) × 10 ⁻²
Homogenized	- 0.978	3.427	4.243
Thermo-mechanically processed	- 0.868	2.96	3.022

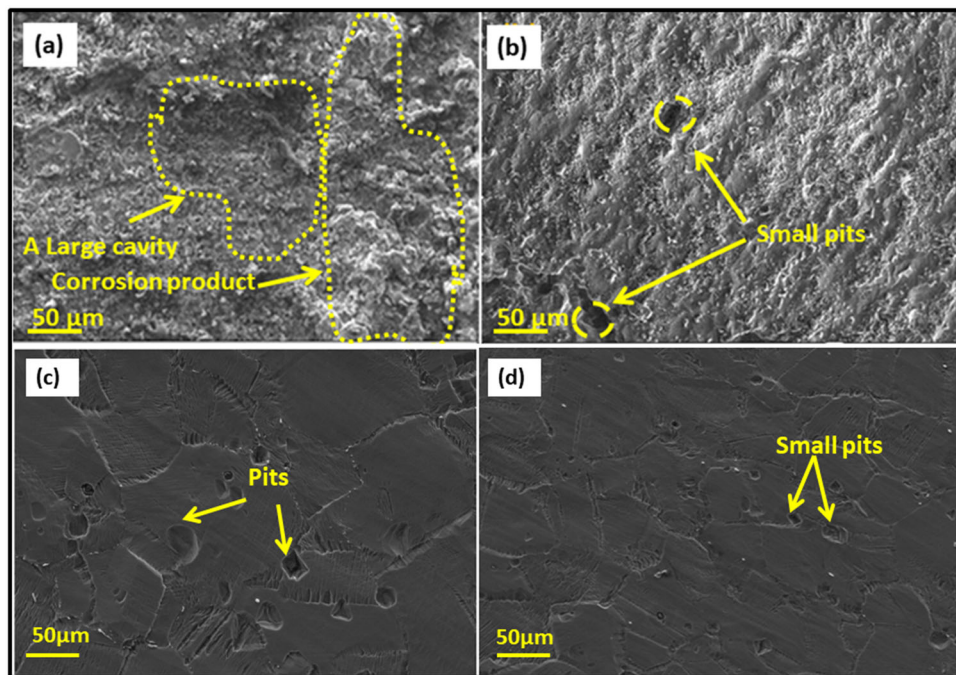


Fig. 8. SEM micrographs (a) homogenized and (b) thermo-mechanically processed HMSMC sample surface after corrosion and (c) homogenized and (d) thermo-mechanically processed HMSMC sample surface after removal of the corrosion product.

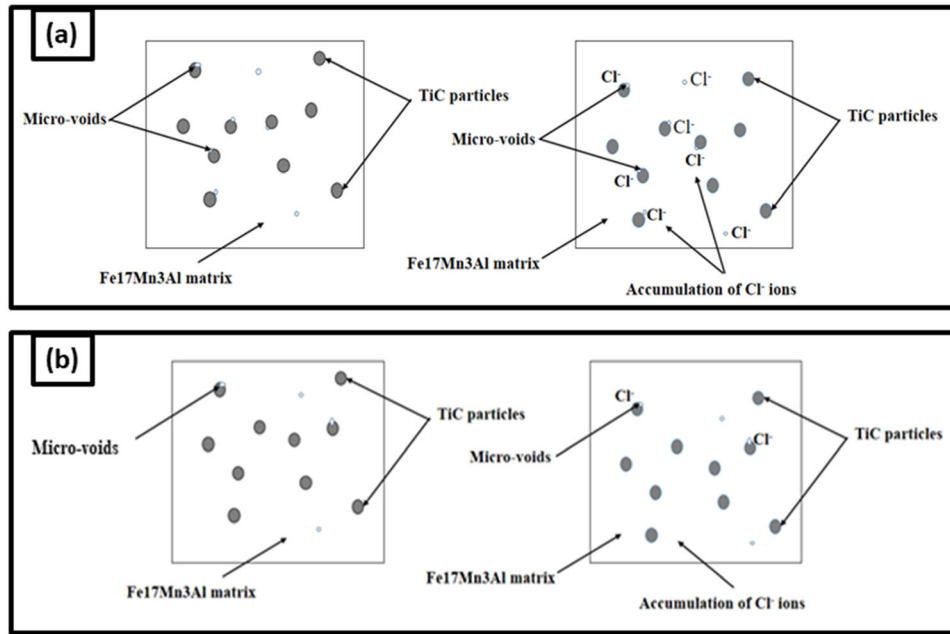


Fig. 9. Mechanism of corrosion process in the (a) homogenized and (b) thermo–mechanically processed HMSMC sample.

particle interface due to the lower concentration of oxygen, which starts the corrosion process and then expands to the other areas of the sample surface. Figure 9b shows the HMSMC sample after the thermo–mechanical processing with only a few microvoids. Therefore, the Cl^- ion accumulation is less than in the homogenized sample. Hence, it takes more time to start and expand the corrosion process.

CONCLUSIONS

The effect of thermo–mechanical processing on the microstructure, impact abrasion wear, and corrosion resistance properties of a high-manganese steel matrix composite (HMSMC) containing 10 wt.% TiC, 3 wt.% Al, and 17 wt.% Mn has been thoroughly studied and the following findings obtained:

- I. The homogenized and thermo–mechanically processed HMSMC samples consist of inter-dendritic and dendritic regions.
- II. The XRD analysis revealed the presence of α -ferrite, γ -austenite, and TiC particles for both the composite samples.
- III. Ferrite is present in the inter-dendritic region, whereas austenite is present in the dendritic region. However, the inter-dendritic region comprises large TiC particles while the dendritic region possesses tiny TiC particles.
- IV. The removal of pores through thermo–mechanical processing increases the density of the HMSMC. The IAW resistance of the HMSMC samples is enhanced by thermal–mechanical processing as a result of a 22 HV increase in hardness. The increased density is

the primary cause of this hardness improvement.

- V. Thermo–mechanical processing provides higher corrosion resistance than homogenized HMSMC by closing up the microvoids or pores.

ACKNOWLEDGEMENTS

The authors acknowledge the Indian Institute of Technology, Kharagpur for providing the research facilities for the present work.

CONFLICT OF INTEREST

The author declare that they have no conflict of interest.

REFERENCES

1. A.K. Srivastava and K. Das, *Mater. Sci. Eng. A* 516, 1 <https://doi.org/10.1016/j.msea.2009.04.041> (2009).
2. R. Dalai, S. Das, and K. Das, *Wear* 420–421, 176 <https://doi.org/10.1016/j.wear.2018.10.013> (2019).
3. S. Mishra and R. Dalai, *Mater. Today: Proc.* 44, 2571 <https://doi.org/10.1016/j.matpr.2020.12.602> (2021).
4. H.Y. Wang, Q.C. Jiang, X.L. Li, and F. Zhao, *J. Alloys Compd.* 366, L9 [https://doi.org/10.1016/S0925-8388\(03\)00737-0](https://doi.org/10.1016/S0925-8388(03)00737-0) (2004).
5. A.K. Srivastava and K. Das, *ISIJ Intern.* 49, 1372 <https://doi.org/10.2355/isijinternational.49.1372> (2009).
6. A.K. Srivastava and K. Das, *Tribol. Intern.* 43, 944 <https://doi.org/10.1016/j.triboint.2009.12.057> (2010).
7. Y. Ma and X. Li, *J. Iron Steel Res. Int.* 19, 60 [https://doi.org/10.1016/S1006-706X\(12\)60114-9](https://doi.org/10.1016/S1006-706X(12)60114-9) (2012).
8. Z. Wang, T. Lin, X. He, H. Shao, J. Zheng, and X. Qu, *J. Alloys Compd.* 650, 918 <https://doi.org/10.1016/j.jallcom.2015.08.047> (2015).
9. S.W. Hu, Y.G. Zhao, Z. Wang, Y.G. Li, and Q.C. Jiang, *Mater. Des.* 44, 340 <https://doi.org/10.1016/j.matdes.2012.07.063> (2013).

10. W. Bleck, *Int. J. Miner. Metall. Mater.* 28, 782 <https://doi.org/10.1007/s12613-020-2166-1> (2021).
11. Z. Wang, T. Lin, X. He, H. Shao, Bo. Tang, and Qu. Xuanhui, *Int. J. Refrac. Met. Hard Mater.* 58, 14 <https://doi.org/10.1016/j.jrmhm.2016.03.013> (2016).
12. G.S. Zhang, J.D. Xing, and Y.M. Gao, *Wear* 260, 728 <http://doi.org/10.1016/j.wear.2005.04.010> (2006).
13. H.J. Song and G.S. Zhang, *Found. Tech.* 26, 468 (2005).
14. E.G. Moghaddam, N. Karimzadeh, N. Varahram, and P. Davami, *Mater. Sci. Eng.: A* 585, 422 <https://doi.org/10.1016/j.msea.2013.07.082> (2013).
15. Y. Ma, X. Li, C. Wang, and L. Lu, *J. Iron Steel Res. Int.* 19, 60 [https://doi.org/10.1016/S1006-706X\(12\)60114-9](https://doi.org/10.1016/S1006-706X(12)60114-9) (2012).
16. R. Dalai, S. Das, and K. Das, *Canad. Metal. Quart.* 53, 317 <https://doi.org/10.1179/1879139514Y.0000000140> (2014).
17. Z.C. Luo, J.P. Ning, J. Wang, and K.H. Zheng, *Wear* 432–433, 1 <https://doi.org/10.1016/j.wear.2019.202970> (2019).
18. F. Qiu, H. Zhang, C. Li, Z. Wang, F. Chang, H. Yang, C. Li, X. Han, and Q. Jiang, *Mater. Sci. Eng. A* 819, 141485 <https://doi.org/10.1016/j.msea.2021.141485> (2021).
19. B. AlMangour, D. Grzesiak, and J.-M. Yang, *Mater. Des.* 96, 150 <https://doi.org/10.1016/j.matdes.2016.02.022> (2016).
20. B.K. Zuidema, D.K. Subramanyam, and W.C. Leslie, *Metall. Mater. Trans. A* 18, 1629 <https://doi.org/10.1007/BF02646146> (1987).
21. M. Abbasi, S. Kheirandish, Y. Kharrazi, and J. Hejazi, *Mater. Sci. Eng.: A* 513, 72 <https://doi.org/10.1016/j.msea.2009.02.023> (2009).
22. S. Su Sohn, S. Hong, J. Lee, B.C. Suh, S.K. Kim, B.J. Lee, N.J. Kim, and S. Lee, *Acta Mater* 100, 39 <https://doi.org/10.1016/j.actamat.2015.08.027> (2015).
23. M. Abbasi, S. Kheirandish, Y. Kharrazi, and J. Hejazi, *Wear* 268, 202 <https://doi.org/10.1016/j.wear.2009.07.010> (2010).
24. S. Chen, R. Rana, A. Halder, and R.K. Ray, *Prog. Mater. Sci.* 89, 345 <https://doi.org/10.1016/j.pmatsci.2017.05.002> (2017).
25. R. Dalai, S. Das, and K. Das, *Int. J. Miner. Metall. Mater.* 26, 64 <https://doi.org/10.1007/s12613-019-1710-3> (2019).
26. A.K. Srivastava, K. Das, and S. Kr Toor, *Open J. Metal* 5, 11 <https://doi.org/10.4236/ojmetal.2015.52002> (2015).
27. A.K. Srivastava, K. Das, S. Kr-Toor, and K. Sugimoto, *Metallogr. Microstruct. Anal.* 4, 371 <https://doi.org/10.1007/s13632-015-0213-5> (2015).
28. J. Bosch, U. Martin, W. Aperador, J.M. Bastidas, J. Ress, and D.M. Bastidas, *Materials* 14, 425 <https://doi.org/10.3390/ma14020425> (2021).
29. F.C. Ma, W.J. Lu, J.N. Qin, and D. Zhang, *Mater. Trans.* 47, 1322 <https://doi.org/10.2320/matertrans.47.1322> (2006).
30. R.N. Rai, A.K. Prasada Rao, G.L. Dutta, and M. Chakraborty, *Mater. Sci. Forum.* 765, 418 <https://doi.org/10.4028/www.scientific.net/MSF.765.418> (2013).
31. Q. Wu, Y. Sun, C. Yang, F. Xue, and F. Song, *Mater. Trans.* 47, 2393 <https://doi.org/10.2320/matertrans.47.2393> (2006).
32. R. Thimmarayan and G. Thanigaiyarasu, *Int. J. Adv. Manuf. Tech.* 48, 625 <https://doi.org/10.1007/s00170-009-2316-0> (2010).
33. S. Mohapatra, D. Palai, B. Satpathy, S. Das, and K. Das, *Mater. Today Commun.* 34, 105282 <https://doi.org/10.1016/j.mtcomm.2022.105282> (2023).
34. Z. Liu and H. Fredriksson, *Metall. Mater. Trans. A* 28, 707 (1997).
35. O. Kubashevski and C.B. Alcock, *Metallurgical thermochemistry*, 5th edn. (Pergamon, Elmsford, NY, 1979).
36. G.K. Sigworth and J.F. Elliott, *Metal Sci.* 8, 298 <https://doi.org/10.1179/msc.1974.8.1.298> (1974).
37. X. Wang, X. Song, Y. Chen, Z. Wang, and L. Zhang, *Int. J. Electrochem. Sci.* 13, 6436 <https://doi.org/10.20964/2018.07.12> (2018).
38. J. Nie, F. Wang, Y. Chen, Q. Mao, H. Yang, Z. Song, X. Liu, and Y. Zhao, Microstructure and corrosion behavior of Al-TiB₂/TiC composites processed by hot rolling. *Results Phys.* 14, 102471 <https://doi.org/10.1016/j.rinp.2019.102471> (2019).
39. M.B. Kannan, R.K.S. Raman, and S. Khoddam, *Corr. Sci.* 50, 2879 <https://doi.org/10.1016/j.corsci.2008.07.024> (2008).
40. Y.S. Zhang and X.M. Zhu, *Corr. Sci.* 41, 817 [https://doi.org/10.1016/S0010-938X\(99\)00017-7](https://doi.org/10.1016/S0010-938X(99)00017-7) (1999).
41. Y. Wang, G. Cheng, W. Wu, Q. Qiao, Y. Li, and X. Li, *Appl. Sur. Sci.* 349, 746 <https://doi.org/10.1016/j.apsusc.2015.05.053> (2015).

Publisher's Note Springer Nature remains neutral with regard to jurisdictional claims in published maps and institutional affiliations.

Springer Nature or its licensor (e.g. a society or other partner) holds exclusive rights to this article under a publishing agreement with the author(s) or other rightsholder(s); author self-archiving of the accepted manuscript version of this article is solely governed by the terms of such publishing agreement and applicable law.